

# Mini-modeling and 3D conventional modeling of Fort McMurray geostatistical data

Eugene Ben-Awuah, Samira Kalantari, and Hessameddin Eivazy  
Mining Optimization Laboratory (MOL)  
University of Alberta, Edmonton, Canada

## Abstract

*In this paper, two modeling works performed on the provided geostatistical data related to Fort McMurray formation are elaborated. There are two main steps for regional modeling of reservoir known as mini-modeling and 3-D conventional data modeling. The focus of mini-modeling and 3-D conventional modeling is to model the porosity and permeability throughout the domain in 2-D and 3-D. Various steps of these modeling works are explained in great detail.*

## 1. Introduction

The provided data is from one part of the McMurray formation and consists of 37 wells with information on X-coordinate, Y-coordinate, SZ, elevation from sea level, facies, porosity, and oil saturation for each well. There are 7 different facies (1 to 7) as follows:

- 1 for Sand
- 2 for sandy IHS
- 3 for Muddy IHS
- 4 for Mud at the top
- 5 for Breccia
- 6 for Mud plug
- 7 for Mud at the bottom

In order to visualize the data in 2D, the Locmap program of the GSLIB software is used (Deutsch and Journel, 1997). Fig. 1 shows the location map of the 37 wells in 2D. In Fig. 1, the different colors are used as the means to differentiate the various facies.

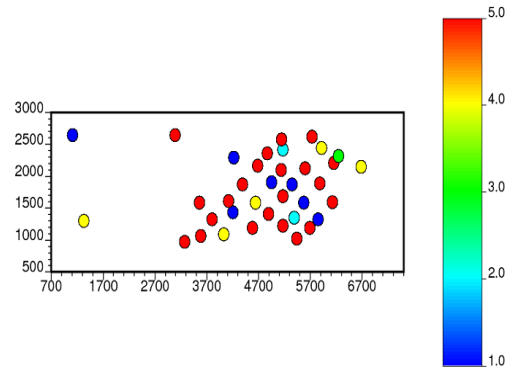


Fig. 1. Location map of the wells (separated by facies).

The organization of this paper is as follows: in section 2, different steps of mini-modeling are elaborated. Section 3 concentrates on the 3-D conventional modeling. Finally, the conclusion is presented in section 4.

## 2. Mini-modeling

Changing the scale from small scale (decimeter scale) to the geological scale is done by mini-modeling. Mini-modeling includes four steps: (1) finding the distribution of porosity by considering well log porosity, (2) modeling porosity-permeability relations, (3) considering the effective permeability values in horizontal and vertical direction and (4) checking the results from the previous steps for geological modeling (Deutsch, 2009). Here, the results of micro-modeling are used to build the mini models.

The main goal of mini-modeling is to establish the porosity/permeability statistics and models for sandy IHS; the resolution is 1dm by 1 dm by 1dm within a volume of 1m by 1m by 1m. Several realizations are done to simulate the porosity values for the mini-modeling grid cells. The probability field simulation and cloud transformation are done to assign the permeability values to the mini-modeling grid cells. In order to find the vertical permeability for the mini model, the  $K_v/K_H$  ratio from micro-modeling results are used. Also, to upscale the data from decimeters to meters; flow simulation is done using the simulation output of porosity values, cloud transformation outputs of horizontal and vertical permeability in order to find the effective porosity and effective horizontal and vertical permeability for the mini-modeling data.

### 2.1. Statistics

After the general description about the mini-modeling goals and tasks to be done, here are some statistics related to the given data, i.e. the maximum, minimum, the mean and the standard deviation (STD) of some variables, are presented in Table 1. showing their histograms.

Table 1. Statistics about the geographical information of data.

Variable	Min.	Max.	Mean	Standard deviation
X-coordinate (m)	1099.6	6678.1	4772.1	1235.66
Y-coordinate (m)	972.2	2643.5	1770.9	517.8
SZ (m)	-77.3	-6.2	-38.6	17.8
Porosity	0.0	0.647	0.208	0.146

Regarding the facies, Table 2 presents the statistics about the porosity for different facies. The following table and plots indicate a summary of statistics and histogram plots of porosity for

different facies. In addition, Figs. 2 to 6 show the histogram plots of porosity values in different facies.

Table 2. Statistics related to facies.

Variable	Facies 1 (sand)	Facies 2 (sandy IHS)	Facies 3 (muddy IHS)	Facies 5 (breccia)	Facies 4, 6 & 7 (muddy shale)
Mean		0.197	0.108	0.203	0.024
Standard deviation	0.074	0.100	0.090	0.091	0.065
Maximum	0.647	0.40	0.38	0.41	0.644
Minimum	0	0	0	0	0

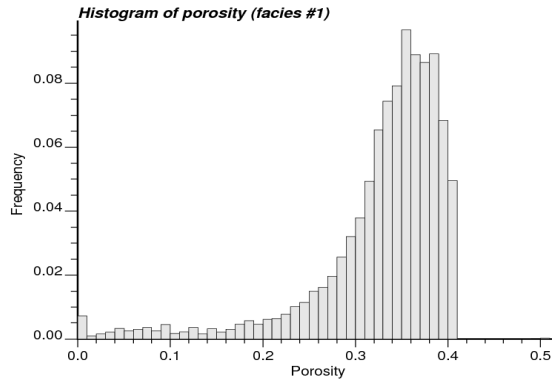


Fig. 2. Histogram plot of porosity of facies 1.

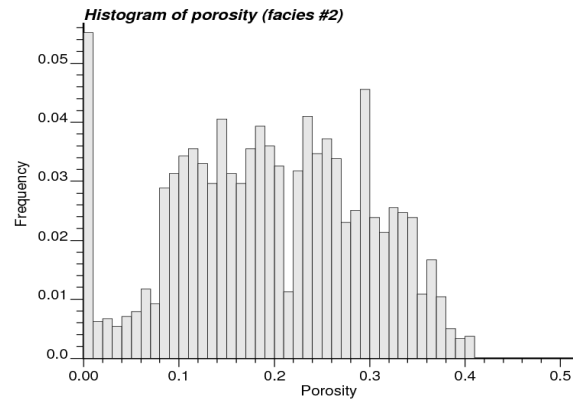


Fig. 3. Histogram plot of porosity of facies 2.

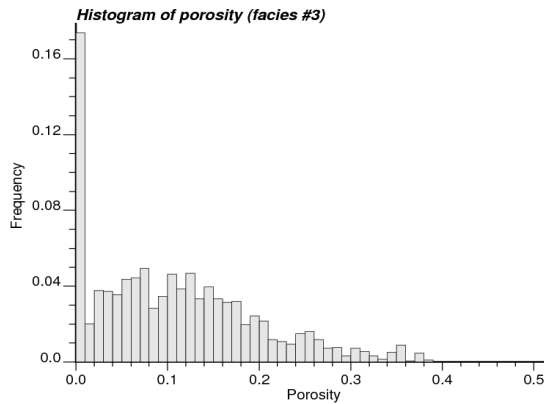


Fig. 4. Histogram plot of porosity of facies 3.

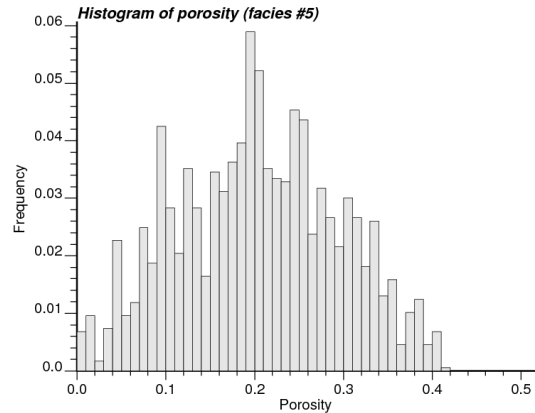


Fig. 5. Histogram plot of porosity of facies 5.

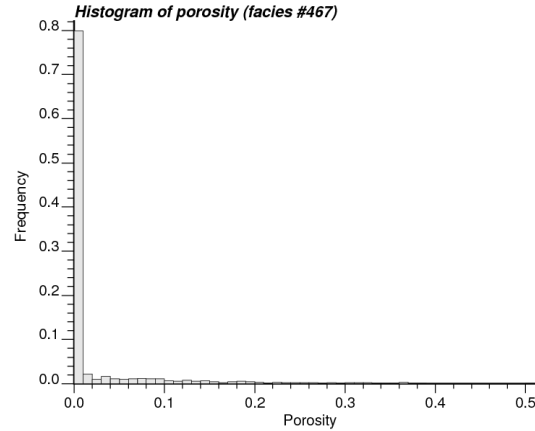


Fig. 6. Histogram plot of porosity of facies 467.

## 2.2. Experimental semivariogram

Experimental semivariogram shows the variability of a variable in a specific direction. To calculate the vertical semivariogram, first, the data are converted to normal score values. This is done using the NSCORE command from GSLIB (Deutsch and Journel, 1997). In this part we are interested in the semivariogram of sandy IHS facies, therefore the data for the sandy HIS facies are used to create the semivariogram. The values of porosity for facies 2 are converted to normal score values. After converting the data, the vertical semivariogram for porosity of facies 2 is calculated based on the corresponding normal score values. Table 3 indicates the parameters for vertical semivariogram calculation.

Table 3. Experimental semivariogram parameters.

Parameter	Value	Parameter	Value
Number of lags	100	Azimuth angle	
Lag separation	0.01m	Dip angle	
Lag tolerance	0.005m	Azimuth tolerance	
Calculation range	1m	Dip tolerance	

## 2.3. Semivariogram modeling

After calculating the experimental semivariogram, it should be modeled. The semivariogram model will be used in simulation, kriging, and other steps of mini-modeling. The specifications of vertical and horizontal semivariogram models are presented in Table 4.

Table 4. Semivariogram model parameters.

Direction	Nested Structure No.	Nested Structure type	Contribution	Range (hor.)
vertical	1	nugget	0.00	N/A
	2	spherical	0.43	0.7 m
	3	spherical	0.57	9.0 m
horizontal	1	nugget	0.00	N/A
	2	spherical	0.43	3.5 m
	3	spherical	0.57	45.0 m

The horizontal semivariogram model is considered to have the same parameters such as nested structure and nugget effect as the vertical semivariogram, but the range of the horizontal

semivariogram is considered to be 5 times the vertical one. Figs. 7 and 8 show the semivariogram models in 2 directions. Here, the value of sill is 1, because the data are normal scores.

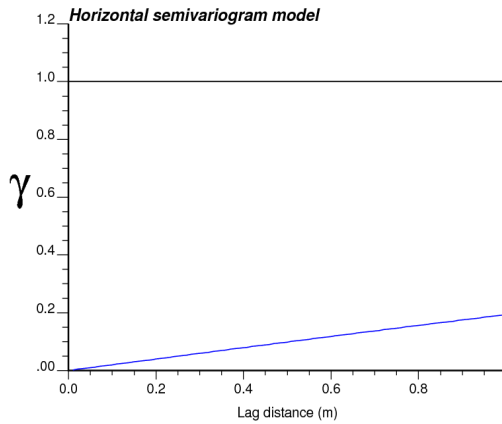


Fig. 7. Semivariogram model in the horizontal direction.

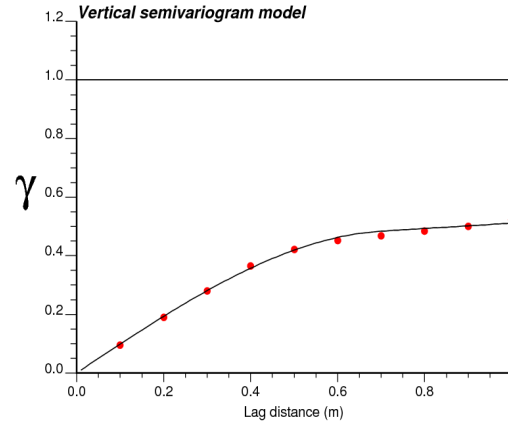


Fig. 8. Semivariogram model in the vertical direction.

#### 2.4. Sequential Gaussian Simulation of Porosity

In this part, porosity of sandy IHS facies is simulated. Two kinds of Gaussian simulation are done on the porosity values, both of them based on unconditional data. One is carried out with no transformation and no reference distribution. The other one is performed with the reference distribution and transformation. The former, is named P-field simulation and its results include the normal scores. In the latter, the transformation is set as the transformation table created in producing the normal scores. Also, the reference distribution is set as the porosity values of facies 2. The results of the latter simulation are in original scale of porosity values. In both kinds of simulation, 100 realizations with grid size of 0.1 m by 0.1 m by 0.1 m along X, Y, and Z directions within the cube of 1m by 1m by 1m are set; therefore there will be 10 grid cells along each direction. Figs. 9 and 10 show the 3-D view of Gaussian simulation of porosity with transformation in original scale after using POSTSIM command of GSLIB for averaging the values of 100 realizations.

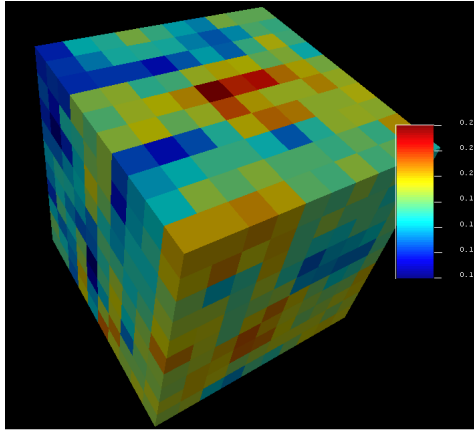


Fig. 9. 3-D view of simulated porosity.

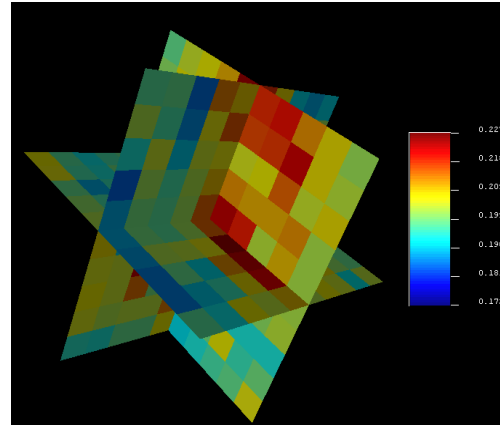


Fig. 10. Typical 2-D views of simulated porosity.

Table 5 indicates the statistics of POSTSIM results.

Table 5. Statistics of results of simulation after using POSTSIM.

Number of lines of the input data	1000
Mean	0.202
Standard deviation	0.007
Minimum	0.185
Maximum	0.22

## 2.5. Bivariate distribution

In order to model the permeability values related to the micro-modeling results, a bivariate distribution of porosity-permeability is required. Using the Bimodel program of GSLIB, the bivariate distribution of porosity and permeability is modeled. Bimodel program quantifies a bivariate distribution at a user-defined discretization for  $K_H$  and  $\emptyset$  (McLennan *et al.*, 2006). The  $K_H$  and  $\emptyset$  were extracted from the flow simulation output of micro-modeling. Fig. 11 indicates the bivariate distribution of porosity and horizontal permeability values.

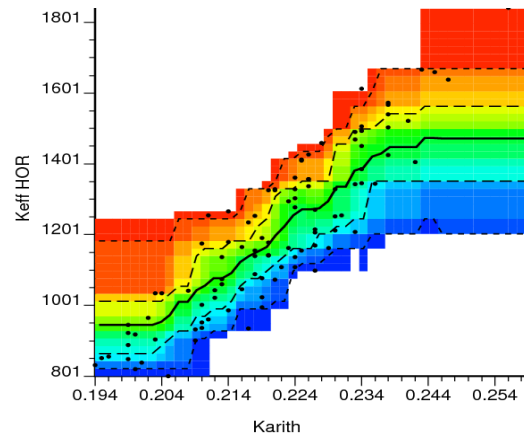


Fig. 11. Bivariate distribution of porosity and horizontal permeability.

## 2.6. Cloud transformation

In this step, to find the horizontal permeability values for the mini-modeling grid cells, the Cltrn program of GSLIB is used. Cloud transformation technique is used to populate the permeability values for the given porosity values from the simulation output. The cloud transformation technique uses the bivariate distribution of porosity and horizontal permeability from micro-modeling results and porosity values of mini-modeling from the sequential Gaussian simulation outputs to assign permeability values to the mini-modeling grid cells. Therefore, three input files for cloud transformation are: the bivariate model of porosity and horizontal permeability from section 2.5 and output files of the 2 types of simulation performed in section 2.4. The output of the cloud transform has three columns: porosity values, probabilities, and K values assigned to the mini-modeling grid cells as the result of cloud transformation. The cloud transform will preserve the uncertainty in the bivariate relationship between porosity and permeability. This technique will use the probability field simulation (p-field) to sample the permeability cumulative distribution function (CDF) to ensure the spatial continuity in the neighboring model cells (Waite *et al.*, 2004). Table 6 represents the statistics for permeability values of cloud transformation results. The output file of cloud transformation includes 100 realizations. Using POSTSIM command, the average of these realizations is obtained. Fig. 12 and Fig. 13 show the output of POSTSIM.

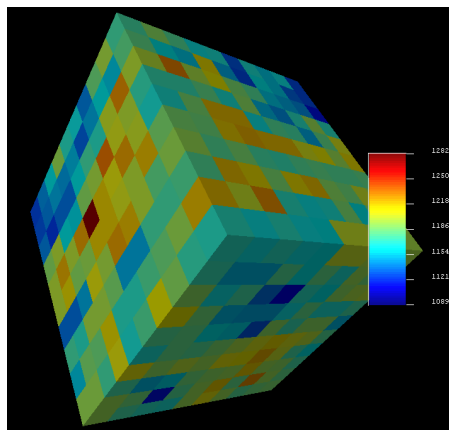


Fig. 12. 3-D view of horizontal permeability from cloud transform.

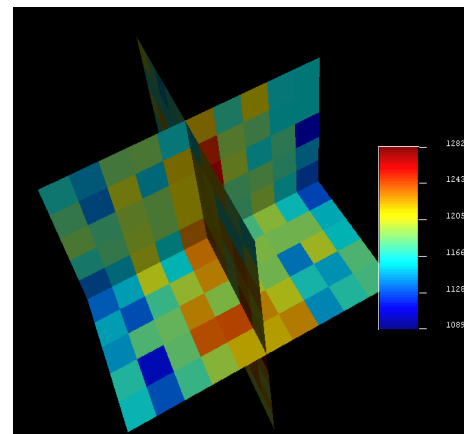


Fig. 13. 2-D views of horizontal permeability from cloud transform.

So far, the bivariate distribution of horizontal permeability and porosity are calculated and drawn. Also, using cloud transformation, the values of horizontal permeability are simulated. There are some ways to calculate the vertical permeability. One way which is applied here is to use the ratio of vertical permeability and horizontal permeability from the flow model done in the macro-modeling. This ratio equals to 1.653. Then, the value of this ratio is multiplied to the values of horizontal permeability outputted from the cloud transform. The results for the vertical permeability are shown in Figs. 14 and 15.

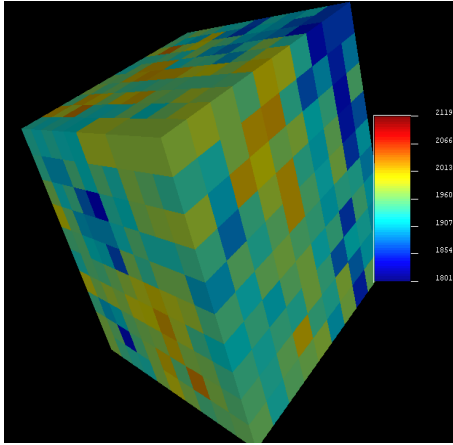


Fig. 14. 3-D view of vertical permeability.

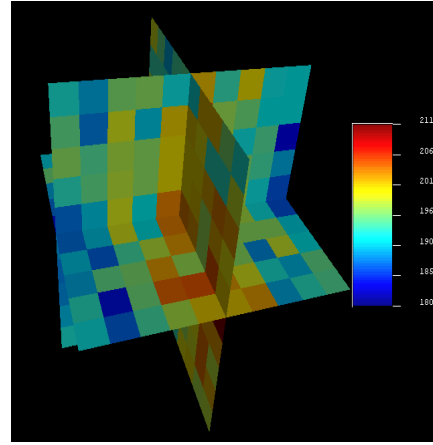


Fig. 15. 2-D views of vertical permeability.

## 2.7. Flow modeling and analysis

Using the porosity, horizontal permeability and vertical permeability from the cloud transformation output, the flow simulation can be done to upscale the data from decimeter scale to the meter scale. The flow simulation calculates the effective horizontal and vertical permeability values and the effective porosity values for the mini-modeling grid cells. Here, using FLOWSIM program of GSLIB, the flow of porosity and permeability in the domain is modeled. The porosity of the domain is calculated as the arithmetic average of porosity of grid cells. The arithmetic average cannot be applied for permeability. The summary statistics of porosity, vertical and horizontal permeability are presented in Table 6.

Table 6. Summary statistics of flow simulation results.

Variable	Min.	Max.	Mean	Standard deviation
Porosity	0.086	0.307	0.1988	0.0449
Vertical permeability (mD)	1554.317	2284.027	1883.0311	176.961
Horizontal permeability (mD)	946.073	1401.500	1161.628	110.856
Vertical/horizontal permeability (mD)	1.592	1.643	1.621	0.0103

Fig. 16 shows the diagram of change of average porosity between 100 realizations of FLOWSIM.



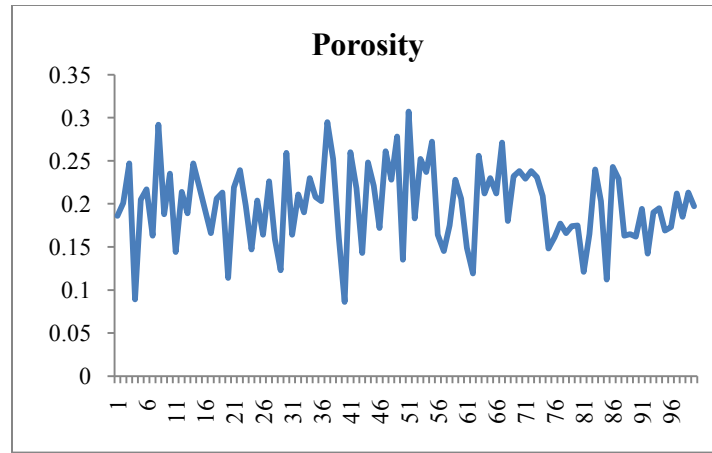


Fig. 16. Diagram of changes of porosity through realizations.

Also, the histograms of porosity, vertical and horizontal permeability are shown in Figs. 17 to 19.

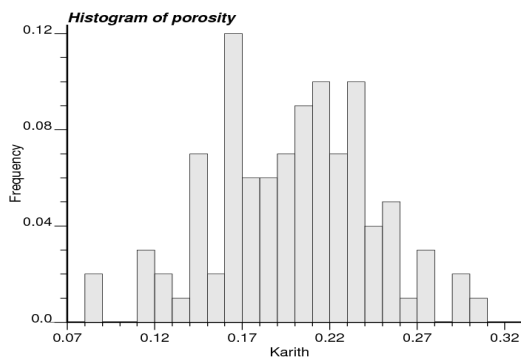


Fig. 17. Histogram plot of porosity.

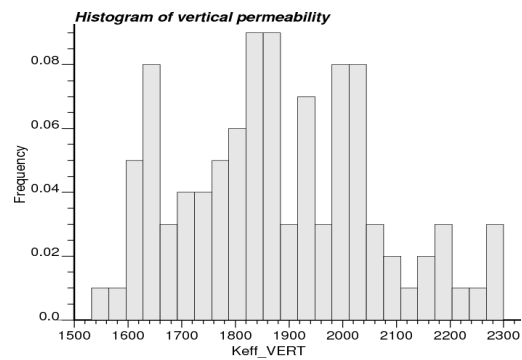


Fig. 18. Histogram plot of vertical permeability.

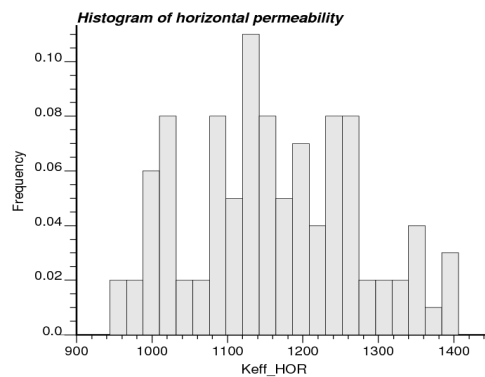


Fig. 19. Histogram plot of horizontal permeability.

Fig. 20 shows the scatter plot of horizontal permeability versus porosity. The correlation is 0.998.

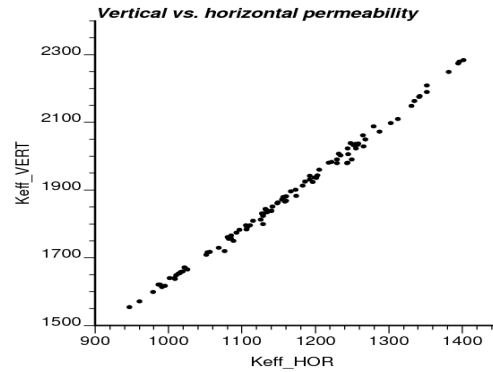


Fig. 20. Scatter plot of vertical permeability versus horizontal permeability.

Fig. 21 shows the scatter plot of the ratio of vertical to horizontal permeability versus horizontal permeability. The corresponding correlation is -0.314.

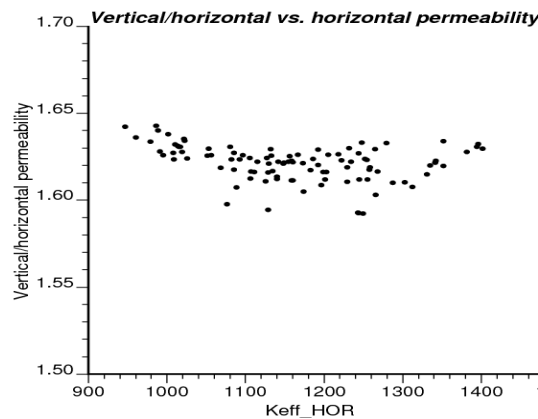


Fig. 21. Scatter plot of ratio of vertical permeability to horizontal permeability versus horizontal permeability.

### 3. 3D conventional modeling

The 3D conventional modeling of an exploration data within the McMurray formation is presented here. Therefore, the general information about the data and the related statistics are the same as in section 2. The steps of the 3D conventional modeling are presented in this section. These steps include facies modeling, porosity modeling and merging the models.

#### 3.1. Facies modeling

The main tasks involved in the facies modeling are as follows: 1) Trend modeling 2) Semivariogram modeling 3) Kriging and 4) Sequential Indicator Simulation (SIS).

##### 3.1.1 Trend modeling

Areal proportions of the facies are summarized by calculating the proportion of each facies in the 37 wells. This gives the facies proportions in all the wells categorized by well ID. Fig. 22 shows the areal proportion of each facies in the vertical direction.

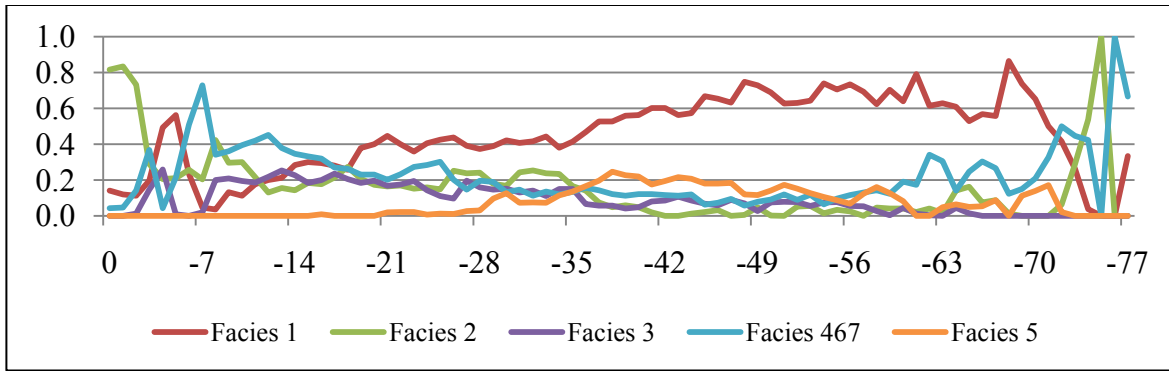


Fig. 22. Areal proportion of each facies in the vertical direction.

Then, in order to estimate the facies trend in 2D at all locations, the facies data are kriged. Ordinary kriging with a variogram that has 40% nugget effect and a range of 1/3 of the domain size is used. This is known as the horizontal trend. The horizontal trend statistics from kriging is summarized in Table 7 for all the facies. Also, Fig. 23 to Fig. 27 show the horizontal trend maps for each facies.

Table 7. Horizontal trend statistics from kriging of all facies.

Parameter \ Statistic	Minimum	Maximum	Mean	Std. deviation
Facies 1	0.264	0.685	0.471	0.095
Facies 2	0.047	0.273	0.134	0.045
Facies 3	0.013	0.283	0.116	0.062
Facies 467	0.066	0.501	0.216	0.089
Facies 5	0.029	0.144	0.064	0.020

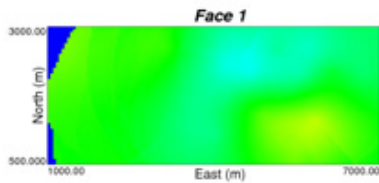


Fig. 23. Horizontal trend map of facies 1.

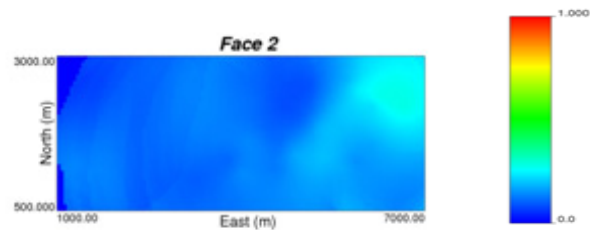


Fig. 24. Horizontal trend map of facies 2.

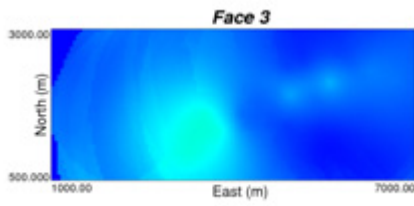


Fig. 25. Horizontal trend map of facies 3.

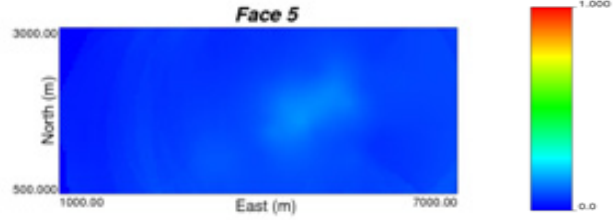


Fig. 26. Horizontal trend map of facies 5.

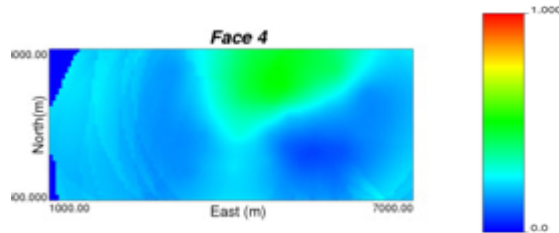


Fig. 27. Horizontal trend map of facies 467.

A vertical trend model is calculated from the data by subsetting the data by slices of SZ. The original vertical data spacing is 0.1m and this is regrouped in SZ slices of 1m which is the target grid dimension. A graph of facies proportion in every 1m depth is plotted to visualize the vertical trend. Fig. 28 to Fig. 32 show the plots of the vertical trend for all of the facies.

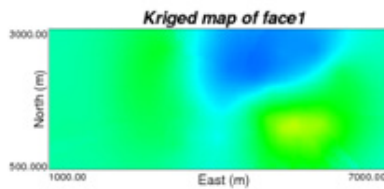


Fig. 28. Vertical trend map of facies 1.

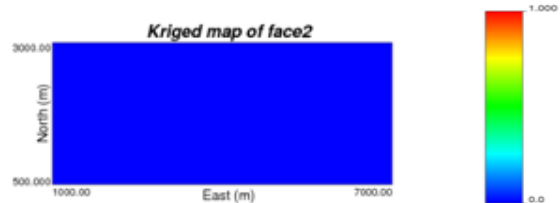


Fig. 29. Vertical trend map of facies 2.



Fig. 30. Vertical trend map of facies 3.

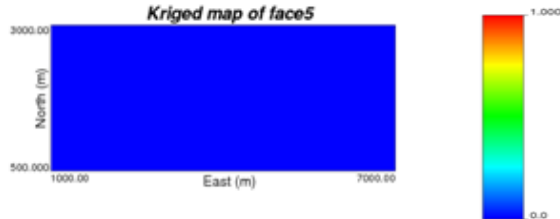


Fig. 31. Vertical trend map of facies 5.

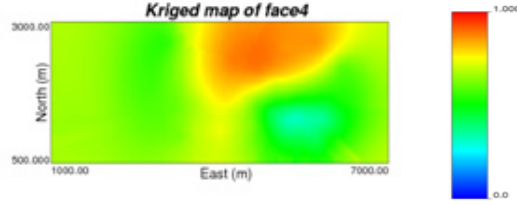


Fig. 32. Vertical trend map of facies 467.

The horizontal and vertical trend models are merged to get a 3-D trend model which will be used to control kriging and simulation of the facies proportion in the grid. The 3-D trend model is calculated based on Eq. (1) (Hong and Deutsch, 2009):

$$m(x, y, z) = \frac{m_z(z) \cdot m_{x,y}(x, y)}{m_{global}} \quad (1)$$

Where  $m_z(z)$ : mean from the vertical trend,

$m_{x,y}(x,y)$ : mean from the areal trend,

$m_{global}$  : global mean from histogram,

$m(x,y,z)$ : mean at location  $(x,y,z)$ .

This equation is based on the assumption of conditional independence of vertical and areal trends. Use of this equation amounts to scaling the vertical trend curve,  $m_z$ , by the areal trend,  $m_x$  and  $m_y$ . Maps of facies of the same slice in the 3D trend model are comparable to that from the 2D trend model.

### 3.1.2 Semivariogram modeling

The original 3-D data is used to calculate the indicator experimental semivariogram for each of the facies in the vertical and horizontal directions. All the vertical semivariograms are modeled from the experimental semivariogram. The horizontal semivariograms for facies 1 and 4 are modeled whilst anisotropy ratio is used to obtain the horizontal semivariogram models for facies 2, 3, and 5. Vertical to horizontal anisotropy ratio is considered to be 1:80. The semivariograms for facies 1 to 5 are shown by Eqs. (2) to (6), respectively. The modeled semivariogram plots are shown in Fig. 33 to Fig. 39.

$$\gamma(h) = 0.0 + 0.125 \text{Exp}_{\substack{av=2.2 \\ ah1=1.0 \\ ah2=1.0}}(h) + 0.103 \text{Sph}_{\substack{av=24.0 \\ ah1=1200.0 \\ ah2=1200.0}}(h) + 0.020 \text{Sph}_{\substack{av=24.0 \\ ah1=20000.0 \\ ah2=20000.0}}(h) \quad (2)$$

$$\gamma(h) = 0.0 + 0.0780 \text{Exp}_{\substack{av=2.5 \\ ah1=200.0 \\ ah2=200.0}}(h) + 0.0487 \text{Sph}_{\substack{av=24.0 \\ ah1=1920.0 \\ ah2=1920.0}}(h) \quad (3)$$

$$\gamma(h) = 0.0 + 0.0500 \text{Exp}_{\substack{av=2.3 \\ ah1=1.0 \\ ah2=1.0}}(h) + 0.0350 \text{Sph}_{\substack{av=10.0 \\ ah1=800.0 \\ ah2=800.0}}(h) + 0.0125 \text{Sph}_{\substack{av=50.0 \\ ah1=4000.0 \\ ah2=4000.0}}(h) \quad (4)$$

$$\gamma(h) = 0.0 + 0.060 \text{Exp}_{\substack{av=1.5 \\ ah1=1.0 \\ ah2=1.0}}(h) + 0.047 \text{Sph}_{\substack{av=7.5 \\ ah1=500.0 \\ ah2=500.0}}(h) + 0.055 \text{Sph}_{\substack{av=60.0 \\ ah1=1400.0 \\ ah2=1400.0}}(h) \quad (5)$$

$$\gamma(h) = 0.0 + 0.0553 \text{Exp}_{\substack{av=2.5 \\ ah1=200.0 \\ ah2=200.0}}(h) + 0.0180 \text{Sph}_{\substack{av=12.0 \\ ah1=960.0 \\ ah2=960.0}}(h) \quad (6)$$

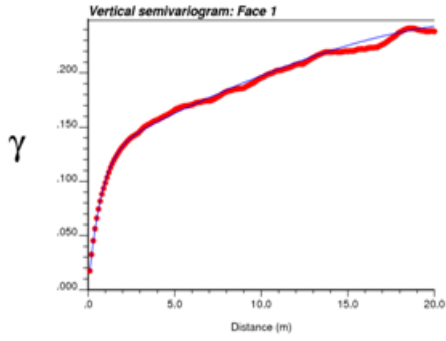


Fig. 33. Vertical semivariogram model of facies 1.

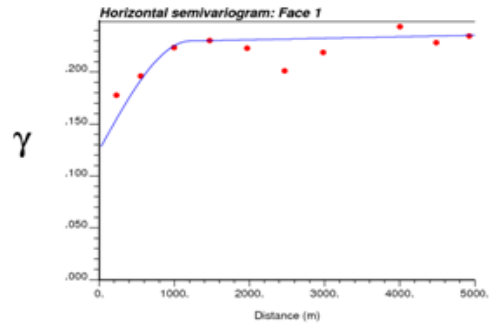


Fig. 34. Horizontal semivariogram model of facies 1.

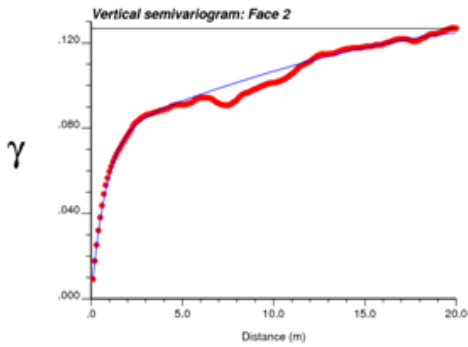


Fig. 35. Vertical semivariogram model of facies 2.

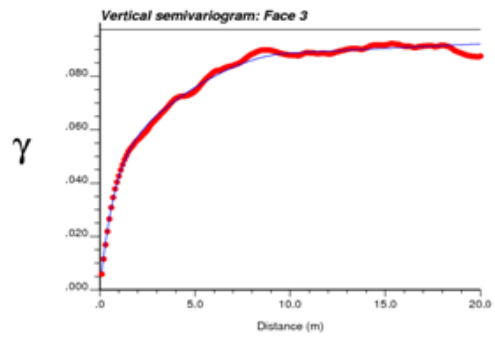


Fig. 36. Vertical semivariogram model of facies 3.

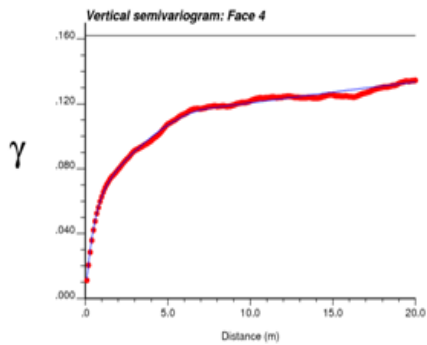


Fig. 37. Vertical semivariogram model of facies 467.

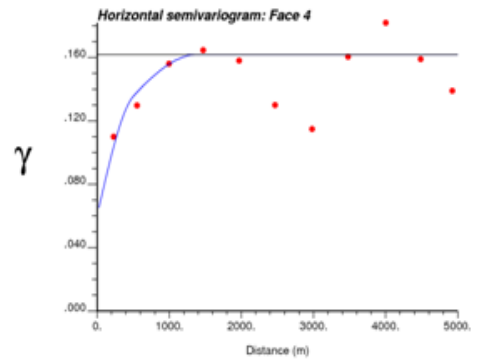


Fig. 38. Horizontal semivariogram model of facies 467.

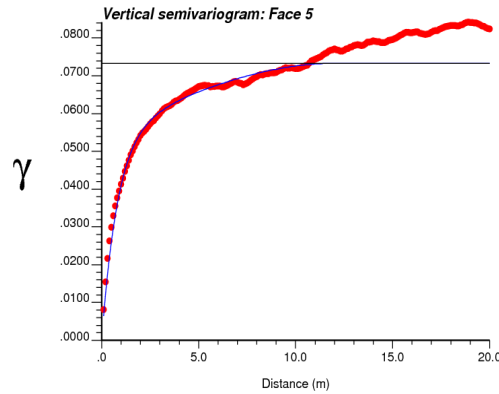


Fig. 39. Vertical semivariogram model of facies 5.

### 3.1.3 Kriging

Using simple kriging, facies kriged model is validated and estimated from the data using the semivariogram models and the 3-D trend model on a grid of blocks, 120 x 50 x 78 with block sizes of 50m in x-y direction and 1m in z direction. The use of the trend model is to guide the kriging process as various facies proportions in the grid. The cross validation of the facies showed good results with high correlation coefficients and a regression slope of 1 in all facies. After kriging 468000 blocks, the estimated mean and standard deviation for the facies have been summarized in Table 8. Figs. 40 to 44 show the kriged maps of the facies.

Table 8. Summary statistics from the kriged facies models

Parameter \ Statistic	Minimum	Maximum	Mean	Std. deviation
Facies 1	0	0.995	0.468	0.224
Facies 2	0	1.000	0.158	0.187
Facies 3	0	0.550	0.099	0.103
Facies 467	0	1.000	0.247	0.182
Facies 5	0	0.376	0.065	0.068

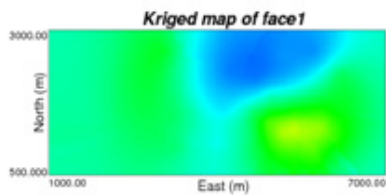
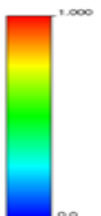


Fig. 40. Kriged map of facies 1.



Fig. 41. Kriged map of facies 2.



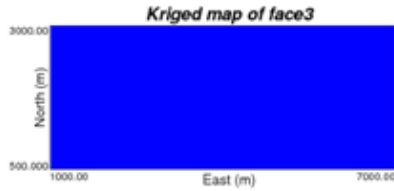


Fig. 42. Kriged map of facies 3.



Fig. 43. Kriged map of facies 5.

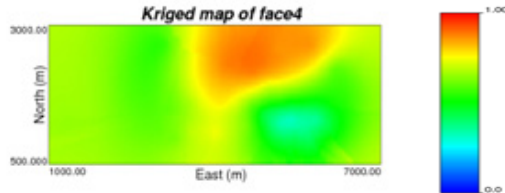
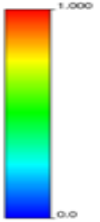


Fig. 44. Kriged map of facies 467.

### 3.1.4 Sequential indicator simulation (SIS)

Using simple kriging with locally varying means (LVM), a facies SIS is performed using the original 3-D well data, the 3-D trend model data and the semivariogram models. The use of the trend model is to guide the simulation process as to the various facies proportions in the grid. 100 realizations are simulated with light cleaning and the results summarized for comparison with the kriged data. The mean and standard deviation of the facies from SIS are shown in Table 9 and compares well with kriged results and the original data statistics. Fig. 45 shows a 2D view of 100 realization from the SIS data which shows the dominance of facies 467 at the upper portion of the formation.

Table 9. Statistics of SIS for each facies.

Parameter	Mean	Std. deviation
Facies 1	0.492	0.480
Facies 2	0.133	0.339
Facies 3	0.086	0.281
Facies 467	0.249	0.432
Facies 5	0.040	0.196



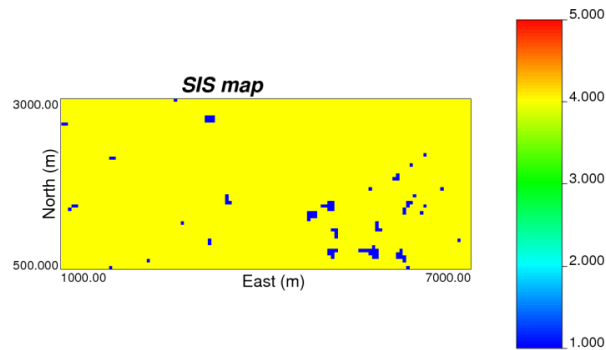


Fig. 45. 2D view of facies model from simulation.

### 3.2. Porosity modeling

The tasks involved in porosity modeling are: 1) declustering and normal score transform 2) semivariogram modeling 3) kriging and 4) Sequential Gaussian Simulation (SGS).

#### 3.2.1 Declustering and normal score transform

The subset porosity data are declustered to quantify the impact of irregular drillhole spacing on the porosity statistics. The results from the declustered data compared with the equal weighted statistics data for each facies is shown in Table 10. There are no significant differences in the two results. The data are then transformed to normal scores without declustered weights to be used in semivariogram and kriging calculations.

Table 10. Statistics of porosity in the facies from equal weighted and declustered data.

Statistic Parameter	Minimum	Maximum	Equal weighted		Declustered	
			Mean	Std. dev.	Mean	Std. dev.
Porosity of facies 1	0	0.647	0.327	0.074	0.311	0.090
Porosity of facies 2	0	0.400	0.197	0.099	0.181	0.103
Porosity of facies 3	0	0.380	0.108	0.089	0.108	0.089
Porosity of facies 467	0	0.644	0.024	0.065	0.024	0.065
Porosity of facies 5	0	0.410	0.203	0.091	0.203	0.091

#### 3.2.2 Semivariogram modeling

The normal score data without declustering weights is used in calculating the experimental semivariograms for each of the facies porosity in the vertical and horizontal directions. All the vertical semivariograms are modeled from the experimental semivariograms. The horizontal semivariograms for porosity of facies 467 is modeled whilst anisotropy ratio is used to obtain the horizontal semivariogram models for porosity of facies 1, 2, 3, and 5. Vertical to horizontal anisotropy ratio of 1:80 is used. The porosity semivariograms for the five facies are modeled by Eq. (7) to (11), respectively. The modeled porosity semivariogram plots are presented in Figs. 46 to 51.

$$\gamma(h) = 0.0 + 0.47 \text{Exp}_{\substack{av=1.2 \\ ah1=96.0 \\ ah2=96.0}}(h) + 0.53 \text{Sph}_{\substack{av=22.0 \\ ah1=1760.0 \\ ah2=1760.0}}(h) \quad (7)$$

$$\gamma(h) = 0.0 + 0.53 \text{Exp}_{\substack{av=1.1 \\ ah1=88.0 \\ ah2=88.0}}(h) + 0.47 \text{Sph}_{\substack{av=24.0 \\ ah1=1920.0 \\ ah2=1920.0}}(h) \quad (8)$$

$$\gamma(h) = 0.0 + 0.51 \text{Exp}_{\substack{av=1.1 \\ ah1=88.0 \\ ah2=88.0}}(h) + 0.49 \text{Sph}_{\substack{av=40.0 \\ ah1=3200.0 \\ ah2=3200.0}}(h) \quad (9)$$

$$\gamma(h) = 0.4 + 0.13 \text{Exp}_{\substack{av=0.1 \\ ah1=1.0 \\ ah2=1.0}}(h) + 0.17 \text{Sph}_{\substack{av=4.0 \\ ah1=1900.0 \\ ah2=1900.0}}(h) + 0.30 \text{Sph}_{\substack{av=40.0 \\ ah1=1900.0 \\ ah2=1900.0}}(h) \quad (10)$$

$$\gamma(h) = 0.0 + 0.8 \text{Exp}_{\substack{av=1.0 \\ ah1=80.0 \\ ah2=80.0}}(h) + 0.2 \text{Sph}_{\substack{av=60.0 \\ ah1=4800.0 \\ ah2=4800.0}}(h) \quad (11)$$

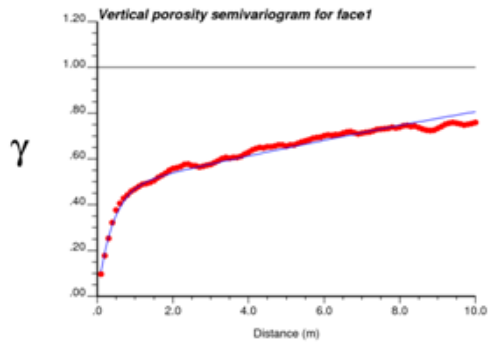


Fig. 46. Vertical semivariogram of porosity for facies 1.

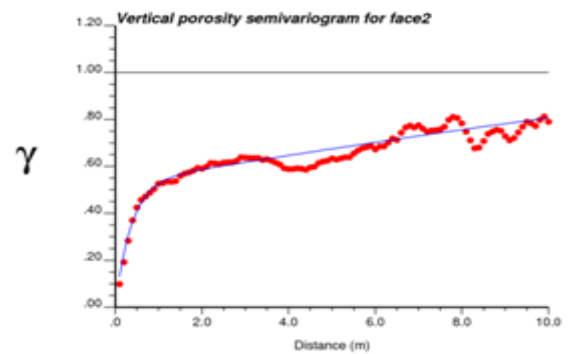


Fig. 47. Vertical semivariogram of porosity for facies 2.

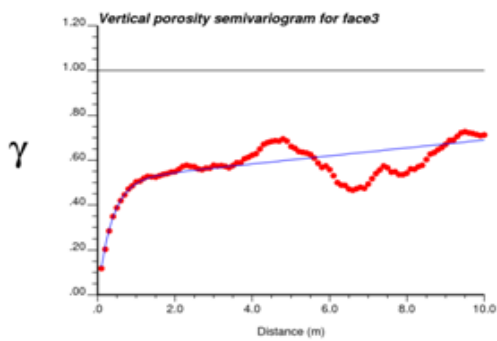


Fig. 48. Vertical semivariogram of porosity for facies 3.

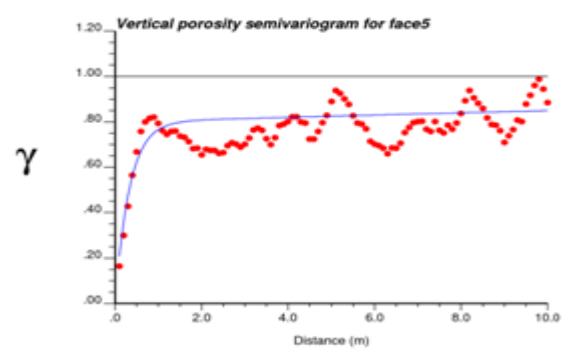


Fig. 49. Horizontal semivariogram of porosity for facies 5.

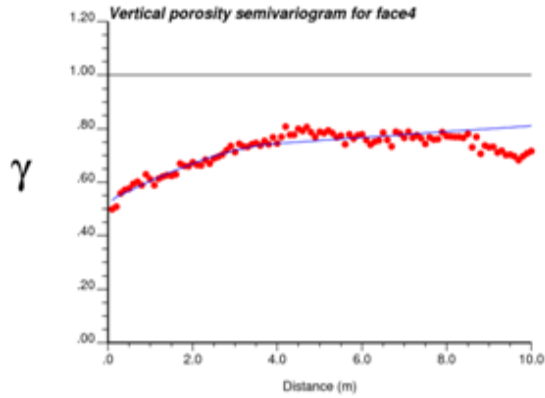


Fig. 50. Vertical semivariogram of porosity for facies 467.

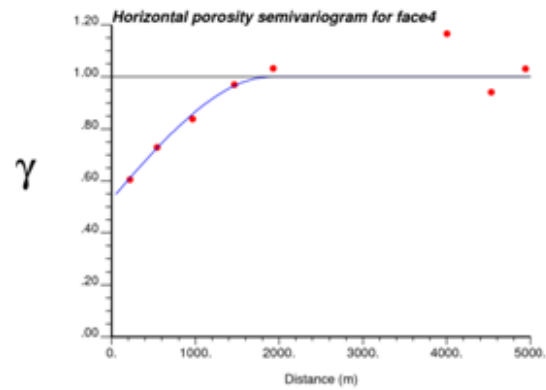


Fig. 51. Horizontal semivariogram of porosity for facies 467.

### 3.2.3 Kriging

Using simple kriging, a porosity kriged model is validated and estimated from the normal score data of each facies using the variogram models on a grid of blocks, 120 x 50 x 78 with block sizes of 50m in x-y direction and 1m in z direction. The cross validation of porosity of the facies shows good results with high correlation coefficients and a slope of regression of 1 in all facies. After kriging 468000 blocks and back-transforming, the estimated mean and variance for porosity of the facies is summarized in Table 11. Figs. 52 to 56 show the cross validation results of porosity of the facies from kriging.

Table 11. Summary statistics from the porosity kriged model of the facies.

Parameter	Minimum	Maximum	Mean	Std. deviation
Kriged porosity of facies1	0.278	0.347	0.344	0.005
Kriged porosity of facies 2	0.000	0.209	0.192	0.013
Kriged porosity of facies 3	0.056	0.151	0.098	0.006
Kriged porosity of facies 467	0.000	0.113	0.011	0.025
Kriged porosity of facies 5	0.000	0.223	0.176	0.068

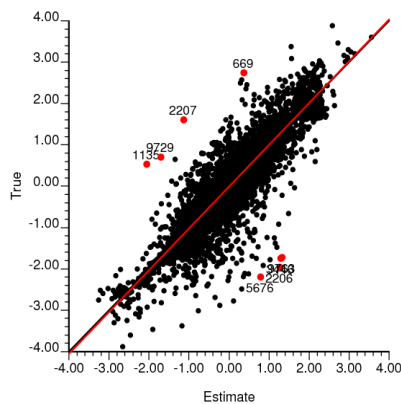


Fig. 52. Cross validation for facies 1.

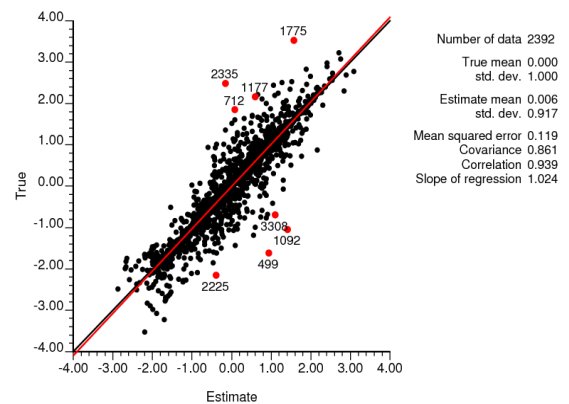


Fig. 53. Cross validation for facies 2.

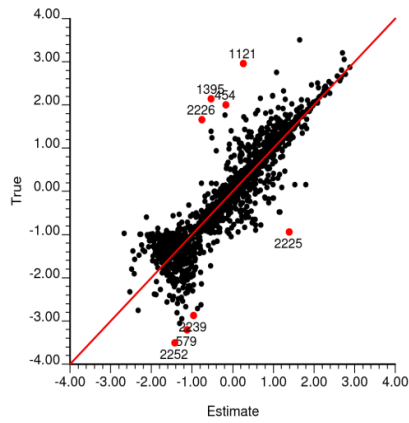


Fig. 54. Cross validation for facies 3.

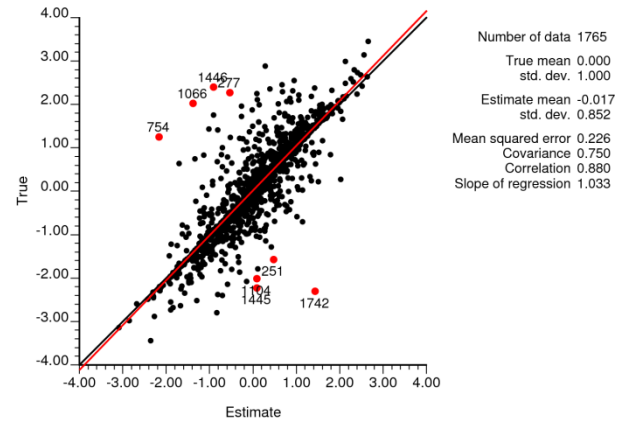


Fig. 55. Cross validation for facies 467.

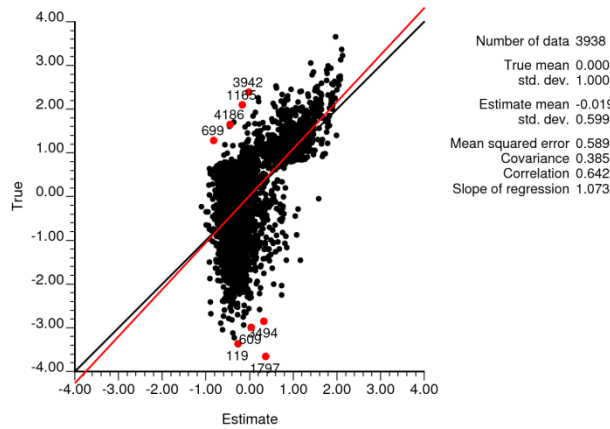


Fig. 56. Cross validation for facies 5.

### 3.2.4 Sequential Gaussian Simulation (SGS)

Using simple kriging a SGS of porosity is performed using the declustered porosity data of each facies and the semivariogram models. The grid system is simulated through 100 realizations and the results are summarized for comparison with the kriged data. The mean and standard deviation of porosity of the facies from SGS are presented in Table 12 and compares well with the kriged results and the original data statistics. Figs. 57 to 61 show the map of porosity of the facies from the SGS data which shows the dominance of porosity of facies 1.

Table 12. Statistics of porosity of the facies from SGS.

Parameter	Minimum	Maximum	Mean	Std. deviation
SGS porosity of facies 1	0	0.364	0.307	0.015
SGS porosity of facies 2	0	0.300	0.177	0.016
SGS porosity of facies 3	0	0.259	0.098	0.015
SGS porosity of facies 467	0	0.210	0.018	0.008
SGS porosity of facies 5	0	0.400	0.202	0.009

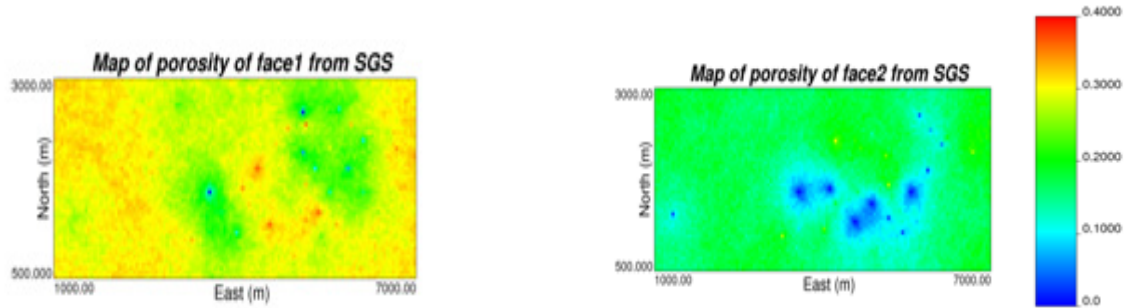


Fig. 57. Simulation map of porosity for facies 1.

Fig. 58. Simulation map of porosity for facies 2.

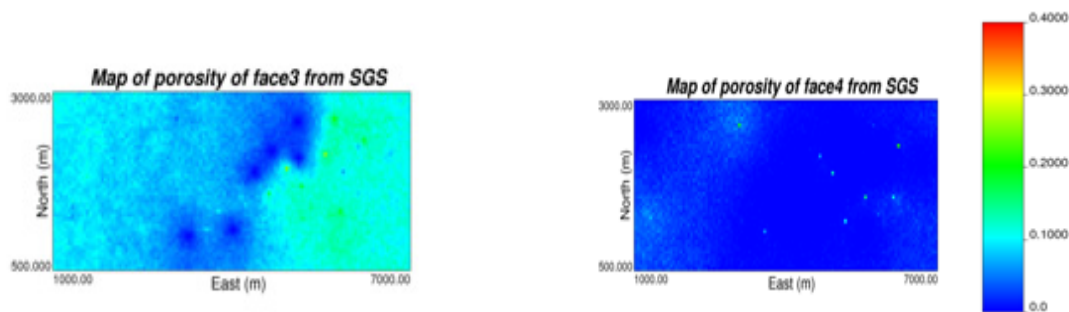


Fig. 59. Simulation map of porosity for facies 3. Fig. 60. Simulation map of porosity for facies 5.

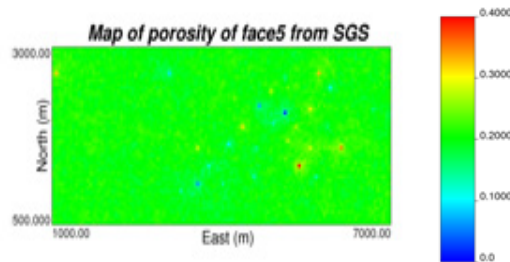


Fig. 61. Simulation map of porosity for facies 467.

### 3.3. Merging models

The facies simulation output from SIS and the five porosity simulation outputs of the facies are merged to get the final 100 porosity models. This is done by matching the different porosity data of the facies with the facies data from simulation and drawing the appropriate porosity value that matches the simulated facies. Statistics from the merged porosity models are summarized in Table 13. The histogram plot of the merged porosity models is shown in Fig. 62. Maps of slice 1 and 78 of 100th realization in the merged porosity models are shown in Fig. 63. This shows the dominance of facies 467 with low porosity values in the upper portion of the formation and facies 1, 2 and 5 with high porosity values in the lower portion of the formation.

Table 13. Statistics from merged porosity models.

Parameter	Minimum	Maximum	Mean	Std. deviation
Porosity of merged model	0	0.647	0.179	0.155

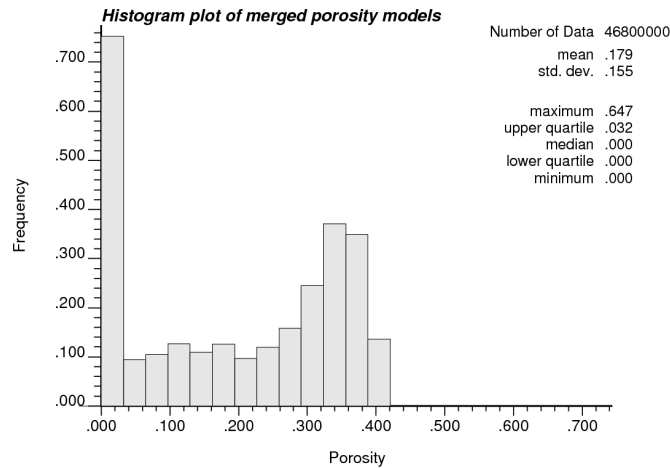


Fig. 62. Histogram plot of the merged porosity models.

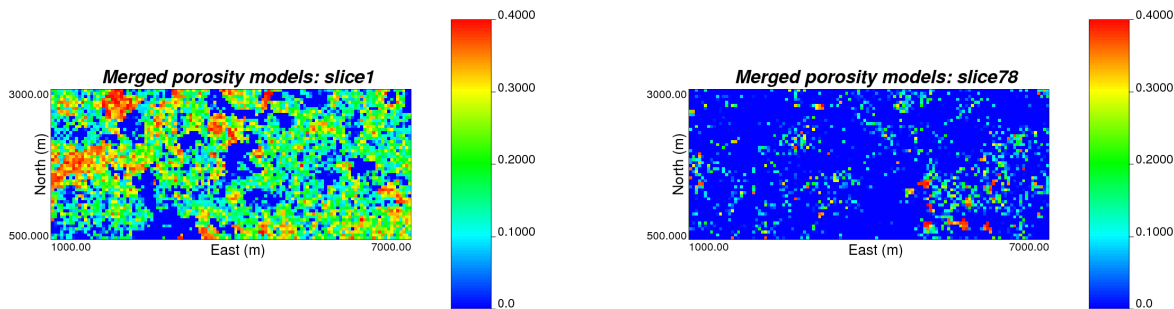


Fig. 63. Maps of slice 1 and 78 of realization 100 in the merged porosity models.

#### 4. Conclusions

In this paper, two main modeling at the scale of regional modeling are performed. The data related to geological features of a domain in Fort McMurray formation are used for these modeling works. Mini-modeling considers the results of micro-modeling and the well log data. The resolution scale is  $dm^3$  within a  $m^3$  volume. Bivariate distribution of porosity-horizontal permeability from the micro-modeling results are extracted. Then, using cloud transformation technique, horizontal permeability values are assigned to the mini-modeling grid cells. In order to find the vertical permeability, the average  $K_v/K_H$  ratio of micro-modeling is used. The correlation between  $K_v/K_H$  ratio and  $K_H$  is very low which is reasonable. On the other hand, the 3-D conventional data modeling enables us to estimate porosity of a deposit at a resolution of about 103m. The five facies in the study area under consideration are: 1) sand, 2) sandy Inclined Heterolithic Strata (IHS), 3) muddy IHS, 4) mud, and 5) breccia. The most dominant facies are 1 and 467. Facies 1 has the most

dominant porosity value of 0.3 and facies 467 is the least porous with a value approximately zero. After merging the facies model and the porosity models, 100 final models of porosity are obtained.

## 5. References

- [1] Deutsch, C. V. (2009). Geostatistical methods for modeling earth sciences data. Edmonton, University of Alberta,
- [2] Deutsch, C. V. and Journel, A. G. (1997). *GSLIB: Geostatistical Software Library and Users Guide*. Oxford University Press, New York, Second ed,
- [3] Hong, S. and Deutsch, C. V. (2009). 3D trend modeling by combining lower order trends. CCG Annual Report 11, University of Alberta, Edmonton,
- [4] McLennan, J. A., Deutsch, C. V., Garner, D., Wheeler, T. J., Richy, J. F., and Mus, E. (2006). Permeability Modeling for SAGD Process Using Minimodels. *Society of Petroleum Engineers*,
- [5] Waite, M., Johanson, S., and Betancourt, D. (2004). *Modeling of Scale-Dependent Permeability Using Single-Well Micro-Models: Application to Hamaca Field, Venezuela*, in Proceedings of SPE International Thermal Operations and Heavy Oil Symposium and Western Regional Meeting, Society of Petroleum Engineers, Bakersfield, California,